DOI: 10.1002/adom.201800395
Article type: Communication

Optical Response of Nano-hole Arrays Filled with Chalcogenide Low-epsilon Media

Davide Piccinotti, Behrad Gholipour, Jin Yao, Kevin F. MacDonald, Brian E. Hayden and Nikolay I. Zheludev*

D. Piccinotti, Dr. B. Gholipour, Prof. K. F. MacDonald, and Prof. N. I. Zheludev
Optoelectronics Research Centre and Centre for Photonic Metamaterials, University of Southampton, Southampton, SO17 1BJ, UK
E-mail: kfm@orc.soton.ac.uk
Dr. B. Gholipour, Dr. J. Yao, and Prof. B. E. Hayden
Department of Chemistry, University of Southampton, Southampton, SO17 1BJ, UK
Prof. N. I. Zheludev
Centre for Disruptive Photonic Technologies & The Photonics Institute, School of Physical and Mathematical Sciences, Nanyang Technological University, Singapore 637371

Keywords: Photonic metamaterial; Chalcogenide; Low-epsilon; Low-index

When an array of subwavelength apertures in a metal film is filled with a chalcogenide semiconductor - a low-epsilon medium at optical frequencies - an increase in transmission over a broad range of plasmonic frequencies is observed, and found to be enabled by 'laminar' flow of energy through the chalcogenide inclusions. For a low-epsilon medium with causality-bound dispersion of the real and imaginary parts of relative permittivity, a peak in transmission emerges at a wavelength tending towards that of unitary refractive index as losses decrease, while counterintuitively the absorption of the composite structure increases.

Nano-structuring can provide an astonishing level of control over the optical properties of a thin metal film: depending on the dimensions and geometric design, one may achieve extraordinarily strong transmission through optically thick films[1-3] or extraordinarily low transmission through optically thin (partially transparent) films.[4-7] Moreover, chiral nano-structuring in metamaterials can lead to optical activity[8, 9] and asymmetric transmission of

polarized light in opposing directions.[10, 11] Metamaterial structuring of dielectric films can lead to the appearance of magnetic optical response,[12] enable the creation of non-reflective "Huygens surfaces",[13] provide for the excitation of toroidal[14] and anapole[15] electromagnetic modes. Very interesting opportunities are also offered by materials presenting an electromagnetic response that lies between those of metals and dielectrics. In semiconductors inter- and intra-band transitions can lead to strong dispersion of optical properties with spectral domains of low and high loss, negative and positive values of the real part of relative permittivity, plasmonic and 'epsilon-near-zero' (ENZ) behaviors and, in some cases, distinctive topologically-protected surface optical properties can be observed.[16] Good examples of such highly dispersive materials are chalcogenide semiconductors - alloys based upon sulfur, selenium or tellurium, wherein dielectric responses of different types can be seen across the visible and near infrared parts of the spectrum and optical properties can be 'engineered' by controlling alloy composition.[16, 17] Chalcogenides have been employed as functional (esp. phase-change) media in active plasmonic metamaterials, wherein they are hybridized with noble metal nanostructures,[18-21] and are now being investigated as material platforms for metamaterials in their own right.[22-24]

Recently Engheta *et al.* have shown that the transmission of sub-wavelength waveguide channels can be enhanced by filling them with zero/low-loss ENZ media, whereby these channels can act as 'wires' for light,[25] in particular in interconnect and 'metatronic' applications.[26] Moreover, a range of exciting and unusual phenomena have been predicted in ENZ materials, including for example control over the relaxation rates of and cooperative interactions between embedded quantum emitters,[27, 28] and "anti-Snell's law" refraction at interfaces with high-permittivity media.[29] Although some proof-of principle experiments in the microwave parts of the spectrum have confirmed predictions of the unusual properties of ENZ media,[30, 31] studies in the optical part of the spectrum are typically precluded by

intrinsic losses.[27, 32] Indeed, while values of the real part of relative permittivity ε_1 equal to zero are not uncommon (e.g. in silicon at 294 nm,[33] chromium at 1.088 μm[34]) but corresponding values of the imaginary part of permittivity ε_2 are typically high. So the question is whether there are circumstances, nanostructural geometries for example, in which materials with sufficiently low values of epsilon can manifest unusual behaviors at optical frequencies. Here we consider the transmission of electromagnetic radiation through subwavelength apertures in a plasmonic metal film - examining whether filling the gaps with an optical-frequency low-epsilon medium enhances their transmission at the epsilon-*nearest*-zero wavelength and how the losses inevitably present in a real low-epsilon medium affect the optical properties of such a composite film.

In what follows, beginning with the example of a real chalcogenide low-epsilon semiconductor - antimony telluride (Sb_2Te_3), we demonstrate that filling the apertures of a nanostructured metal film with such a material leads to more complex behavior than simply an enhancement of transmission. Indeed, in some cases the opposite can occur, with transmission suppressed at wavelengths where epsilon is near to zero while being enhanced at others. The complex changes in the composite's spectral response depend strongly on the interplay between the dispersion of the optical properties of the plasmonic nanostructure and the ENZ medium.

Antimony telluride is a binary chalcogenide alloy - a narrow-gap semiconductor known for its phase-change[35] and thermoelectric properties,[36, 37] and lately attracting interest as a 3D topological insulator.[38, 39] In the UV-VIS spectral range its amorphous form exhibits a plasmonic response – a negative value of the real part ε_1 of relative permittivity, as shown by the ellipsometric data presented in **Figure 1a**, which is obtained for a 30 nm film of Sb_2Te_3 prepared by physical vapor deposition on a silicon substrate through co-evaporation from elemental sources of >6N purity: A base pressure of 1.7×10^{-8} mbar is achieved prior to

deposition and the substrate is held within 10 K of room temperature on a water-cooled platen, at a distance of ~150 mm from the sources, to produce low-stress amorphous films.[40] The composition, i.e. the at.% ratio of 2:3, is confirmed by energy dispersive x-ray spectroscopy.

Of the two $\varepsilon_1 = 0$ crossing points, at wavelengths $\lambda_1 = 253$ nm and $\lambda_2 = 506$ nm, the former is of greater interest because losses (i.e. the value of ε_2) are much lower in the near-UV range. Moreover, in the vicinity of this ε_1 zero-crossing the chalcogenide has a refractive index (**Figure 1b**) close to one. To study how optical transmission through nanoscale apertures is affected by Sb:Te as a near-UV low-epsilon / low-index material, we analyzed the optical properties of metasurfaces comprising arrays of parallel, deeply-subwavelength (10 nm width) slots through a 15 nm thick free-standing aluminum film, filled with amorphous Sb_2Te_3 (**Figure 2a**), and for reference an identical metasurface with empty slots. Full-wave electromagnetic simulations of nano-slot metamaterial structures were performed using the finite element method in COMSOL Multiphysics. Structures are assumed to be free-standing in air and of infinite extent (by virtue of periodic boundary conditions) in the *xy* plane. In the first instance, the model employs ellipsometrically measured material parameters for real Sb_2Te_3 as presented in Figure 1 and parameters for aluminum from Reference [41]. It assumes normally incident, narrow-band, coherent illumination polarized in the *x*-direction (perpendicular to the nano-slots).

It is found (**Figure 2b**) that filling the slots with Sb_2Te_3 brings about a broadband increase in transmission over spectral range extending from below λ_1 almost up to λ_2, and a corresponding decrease in reflectivity, even to longer wavelengths. The increase in transmission at the low-loss UV $\varepsilon_1 = 0$ point λ_1 comparatively modest (an absolute change of <5%) and in fact represents a shallow dip in the broader trend of the Al/ Sb_2Te_3 composite film's transmission spectrum, which is matched by a shallow peak in reflection; larger

increases in transmission are seen at longer wavelengths within antimony telluride's plasmonic ($\varepsilon_1 < 0$) band between λ_1 and λ_2.

The cross-sectional maps of electric field strength and powerflow shown in **Figure 2c** illustrate differences between the metasurface optical response for empty and Sb_2Te_3-filled slots. In an array of empty nano-slots, with no chalcogenide material present, 'whirlpools' of optical energy are formed around the nano-slots at short, near-UV wavelengths, within which powerflow through the open aperture is in the backward direction relative to incident light. Such whirlpools are characteristic of resonant plasmonic nanostructures, having initially been observed around plasmonic nanoparticles.[42] With increasing wavelength, at the $\lambda^* = 380$ nm plasmonic resonance losses and radiation backflow balance the inflow of energy, causing the transmission of the perforated Al film to fall to zero at this wavelength.[4-7] At longer wavelengths still, powerflow whirlpools are reestablished, but with rotation in the opposite direction as to the short wavelength side of the λ^* resonance wavelength. The same inversion of the energy circulation direction is seen as the excitation wavelength is tuned across the plasmonic resonance of a metal nanoparticle.[42]

When the slots are filled with Sb_2Te_3, we observe 'laminar' flow of light through the film at all wavelengths, with minimal local field enhancement; no powerflow whirlpools are seen around the slots. (Here we adopt hydrodynamic terminology, where 'laminar flow' describes a regime characterized by high momentum diffusion and low momentum convection with no turbulence. i.e. no whirlpools.) Light propagates from one side of the slot array to the other with the Sb_2Te_3-filled slots acting as conduits for light in which the magnitude of epsilon $|\varepsilon| = \sqrt{(\varepsilon_1^2 + \epsilon_2^2)}$ is low, i.e. nearer to zero than in aluminum. Transmission gradually decreases with increasing wavelength as losses in Sb:Te increase.

To analyze what could conceivably be achieved with low-loss ENZ materials and to understand the role of losses in the transmission changes induced by filling the nano-slots with chalcogenide, it is instructive to consider the effects of reducing the value of ε_2 at the near-UV ε_1 zero-crossing wavelength λ_1. To this end we employ dispersions of ε_1 and ε_2 for a hypothetical chalcogenide material, derived from those of real Sb_2Te_3 by reduction of optical losses (ε_2) in a manner consistent with Kramers-Kronig relations. (Indeed, any departure from the Kramers-Kronig relations between the real and imaginary parts of permittivity would lead to an unphysical description of the material and related wave phenomena, compromising the fundamental causality of electromagnetism.[43]) The measured spectral dispersion of antimony telluride's relative permittivity is reproduced very well (the dashed 'fit' lines in **Figure 3**) by a single Lorentzian oscillator absorption model[44] (detailed in Supporting Information), with an oscillator energy E_0 of 2.1 eV, a static dielectric constant ε_s of 23, a high-frequency dielectric constant ε_∞ of 3.1, and a broadening factor B of 2.65 eV. These parameters are subsequently adjusted to produce modified dispersion curves (Figure 3a and 3b) for hypothetical low-loss media in which ε_2 is reduced by a given factor at λ_1 while maintaining $\varepsilon_1 = 0$ at both of the (real Sb_2Te_3) zero-crossing wavelengths λ_1 and λ_2. (The oscillator model parameters for each case, and corresponding derived values of effective carrier density n and carrier lifetime τ, are presented in Supporting Information Table 1.)

Figure 4 shows the dispersion of metasurface optical properties when the slots are filled with hypothetical materials having losses (values of ε_2) at λ_1 that are up to 25 times smaller than in vapor-deposited Sb_2Te_3. Intriguingly, the reduction of ε_2 at the $\varepsilon_1 = 0$ wavelength λ_1 actually decreases transmission at this point, rather than increasing it one might anticipate from analytical studies of ideal ENZ media (i.e. based upon the idea that electromagnetic waves may traverse sub-wavelength waveguide channels unimpeded when they are loaded with a low-loss ENZ medium).[25, 30] Indeed, the loss reduction results in the emergence of a

pronounced peak in transmission (dip in reflection) at longer wavelengths where moreover, up to a point, metasurface absorption actually increases as losses in the chalcogenide inclusions decrease - the level of absorption saturates with around a factor of eight reduction in ε_2 while absorption linewidth continues to decrease as ε_2 decreases further. These behaviors are consistent with the recent analytical finding[29] that increased losses can increase electromagnetic wave transmission at unstructured, singular air/ENZ interfaces, by facilitating better impedance matching. In the present case, metasurface transmission is determined by the balance among interfacial transmission and reflection coefficients for and propagation losses within the low-epsilon medium, against the backdrop of the nano-structurally engineered response. The spectral position of the emergent transmission resonance tends towards the wavelength at which the magnitude of refractive index $|N| = \sqrt{(n^2 + k^2)}$ (**Figure 5**) is equal to one, i.e. is matched to the incident medium, as losses decrease.[45] The spectral position of the dip in transmission (peak in reflection) near to λ_1 is similarly a function of refractive index - tracking the wavelength at which $|N|$ is minimized, which in turn is a function of the loss reduction factor.

In summary, we show, using experimentally measured material parameters for vapor deposited antimony telluride (Sb_2Te_3) in a series of numerical simulations, that optical frequency low-epsilon and near-unitary index behaviors may be observed even in the presence of realistic losses. Sub-wavelength slots filled with the amorphous chalcogenide can serve as conduits for the 'laminar flow' transmission of UV-visible light through a plasmonic metal screen: localized enhancement and powerflow 'turbulence' in the optical near-field around open apertures in the screen are suppressed, producing a broadband enhancement of transmission. However, transmission is not strongly enhanced at the low-loss epsilon-nearest-zero wavelength. Indeed a reduction of losses in the chalcogenide is found to suppress transmission at this point and can increase, rather than decrease, metasurface absorption

depending on the magnitude of refractive index and the extent of index matching to the surroundings.

Sb_2Te_3 is just one member of a broad chalcogenide family that includes numerous binary, ternary and quaternary sulfide, selenide and telluride alloys. With compositionally controllable optical properties, they offer a uniquely adaptable, CMOS-compatible material base for low-epsilon and low-index photonics, including applications in such areas as transmission enhancement, wavefront shaping and control of spontaneous emission.

Supporting Information

Supporting Information is available from the Wiley Online Library.

Following a period of embargo, the data from this paper can be obtained from the University of Southampton research repository http://doi.org/10.5258/SOTON/D0243.

Acknowledgements

This work was supported by the Engineering and Physical Sciences Research Council, UK [Projects EP/M009122/1 and EP/N00762X/1], and the Singapore Ministry of Education [grants MOE2011-T3-1-005 and MOE2016-T3-1-006].

Received: ((will be filled in by the editorial staff))

Revised: ((will be filled in by the editorial staff))

Published online: ((will be filled in by the editorial staff))

References

[1] T. W. Ebbesen, H. J. Lezec, H. F. Ghaemi, T. Thio, P. A. Wolff, *Nature* **1998**, *391*, 667.

[2] C. Genet, T. W. Ebbesen, *Nature* **2007**, *445*, 39.

[3] W. L. Barnes, A. Dereux, T. W. Ebbesen, *Nature* **2003**, *424*, 824.

[4] D. Reibold, F. Shao, A. Erdmann, U. Peshel, *Opt. Express* **2009**, *17*, 544.

[5] I. S. Spevak, A. Y. Nikitin, E. V. Bezuglyi, A. Levchenko, A. V. Kats, *Phys. Rev. B* **2009**, *79*, 161406.

[6] J. Braun, B. Gompf, G. Kobiela, M. Dressel, *Phys. Rev. Lett.* **2009**, *103*, 203901.

[7] B. Zeng, Y. Gao, F. J. Bartoli, *Sci. Rep.* **2013**, *3*, 2840.

[8] E. Plum, V. A. Fedotov, A. S. Schwanecke, N. I. Zheludev, Y. Chen, *Appl. Phys. Lett.* **2007**, *90*, 223113.

[9] Y. Ye, S. He, *Appl. Phys. Lett.* **2010**, *96*, 203501.

[10] V. A. Fedotov, P. L. Mladyonov, S. L. Prosvirnin, A. V. Rogacheva, Y. Chen, N. I. Zheludev, *Phys. Rev. Lett.* **2006**, *97*, 167401.

[11] V. A. Fedotov, A. S. Schwanecke, N. I. Zheludev, V. V. Khardikov, S. L. Prosvirnin, *Nano Lett.* **2007**, *7*, 1996

[12] J. Zhang, K. F. MacDonald, N. I. Zheludev, *Opt. Express* **2013**, *21*, 26721.

[13] M. Decker, I. Staude, M. Falkner, J. Dominguez, D. Neshev, I. Brener, T. Pertsch, Y. Kivshar, *Adv. Opt. Mater.* **2015**, *3*, 813

[14] T. Kaelberer, V. A. Fedotov, N. Papasimakis, D. P. Tsai, N. I. Zheludev, *Science* **2010**, *330*, 1510.

[15] N. Papasimakis, V. A. Fedotov, V. Savinov, T. A. Raybould, N. I. Zheludev, *Nat. Mater.* **2016**, *15*, 263.

[16] J. Yin, H. N. S. Krishnamoorthy, G. Adamo, A. M. Dubrovkin, Y. Chong, N. I. Zheludev, C. Soci, *NPG Asia Mater.* **2017**, *9*, e425.

[17] S. Guerin, B. Hayden, D. W. Hewak, C. Vian, *ACS Comb. Sci.* **2017**, *19*, 478.

[18] Z. L. Samson, K. F. MacDonald, F. De Angelis, B. Gholipour, K. Knight, C. C. Huang, E. Di Fabrizio, D. W. Hewak, N. I. Zheludev, *Appl. Phys. Lett.* **2010**, *96*, 143105.

[19] B. Gholipour, J. F. Zhang, K. F. MacDonald, D. W. Hewak, N. I. Zheludev, *Adv. Mater.* **2013**, *25*, 3050.

[20] A. K. U. Michel, D. N. Chigrin, T. W. W. Mass, K. Schonauer, M. Salinga, M. Wuttig, T. Taubner, *Nano Lett.* **2013**, *13*, 3470.

[21] Y. G. Chen, T. S. Kao, B. Ng, X. Li, X. G. Luo, B. Luk'yanchuk, S. A. Maier, M. H. Hong, *Opt. Express* **2013**, *21*, 13691.

[22] A. Karvounis, B. Gholipour, K. F. MacDonald, N. I. Zheludev, *Appl. Phys. Lett.* **2016**, *109*, 051103.

[23] Q. Wang, E. T. F. Rogers, B. Gholipour, C. M. Wang, G. H. Yuan, J. H. Teng, N. I. Zheludev, *Nat. Photonics* **2016**, *10*, 60.

[24] B. Gholipour, A. Karvounis, J. Yin, C. Soci, K. F. MacDonald, N. I. Zheludev, *NPG Asia Mater.* **2018**.

[25] M. Silveirinha, N. Engheta, *Phys. Rev. Lett.* **2006**, *97*, 157403.

[26] Y. Li, I. Liberal, N. Engheta, *J. Opt. Soc. Am. B* **2016**, *33*, A72.

[27] I. Liberal, N. Engheta, *Nat. Photonics* **2017**, *11*, 149.

[28] I. Liberal, N. Engheta, *Proc. Natl. Acad. Sci. USA* **2017**, *114*, 822.

[29] S. Feng, *Phys. Rev. Lett.* **2012**, *108*, 193904.

[30] B. Edwards, A. Alu, M. E. Young, M. Silveirinha, N. Engheta, *Phys. Rev. Lett.* **2008**, *100*, 033903.

[31] I. Liberal, A. M. Mahmoud, Y. Li, B. Edwards, N. Engheta, *Science* **2017**, *355*, 1058.

[32] J. B. Khurgin, *Nat. Nanotechnol.* **2015**, *10*, 2.

[33] D. E. Aspnes, A. A. Studna, *Phys. Rev. B* **1983**, *27*, 985.

[34] P. B. Johnson, R. W. Christy, *Phys. Rev. B* **1974**, *9*, 5056.

[35] S. Zastrow, J. Gooth, T. Boehnert, S. Heiderich, W. Toellner, S. Heimann, S. Schulz, K. Nielsch, *Semicond. Sci. Technol.* **2013**, *28*, 035010.

[36] H. Zou, D. M. Rowe, G. Min, *J. Vac. Sci. Technol. A* **2001**, *19*, 899.

[37] Y. Kim, A. DiVenere, G. K. L. Wong, J. B. Ketterson, S. Cho, J. R. Meyer, *Journal of Applied Physics* **2002**, *91*, 715.

[38] D. Hsieh, Y. Xia, D. Qian, L. Wray, F. Meier, J. H. Dil, J. Osterwalder, L. Patthey, A. V. Fedorov, H. Lin, A. Bansil, D. Grauer, Y. S. Hor, R. J. Cava, M. Z. Hasan, *Phys. Rev. Lett.* **2009**, *103*, 146401.

[39] H. Zhang, C.-X. Liu, X.-L. Qi, X. Dai, Z. Fang, S.-C. Zhang, *Nat. Phys.* **2009**, *5*, 438.

[40] S. Guerin, B. E. Hayden, *J. Comb. Chem.* **2006**, *8*, 66.

[41] K. M. McPeak, S. V. Jayanti, S. J. Kress, S. Meyer, S. Iotti, A. Rossinelli, D. J. Norris, *ACS Photonics* **2015**, *2*, 326.

[42] M. V. Bashevoy, V. A. Fedotov, N. I. Zheludev, *Opt. Express* **2005**, *13*, 8372.

[43] M. H. Javani, M. I. Stockman, *Phys. Rev. Lett.* **2016**, *117*, 107404.

[44] F. Wooten, in *Optical Properties of Solids*, Academic Press, New York and London 1972, 42

[45] R. Maas, J. Parsons, N. Engheta, A. Polman, *Nat. Photonics* **2013**, *7*, 907.

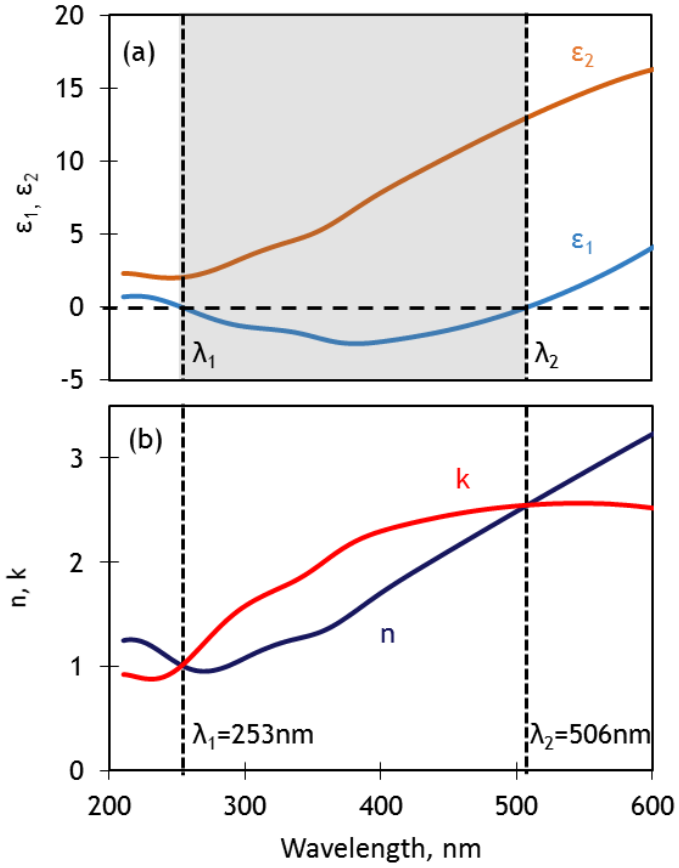

Figure 1. UV-VIS plasmonic and low-epsilon/low-index properties of amorphous antimony telluride. (a) Real [ε_1] and imaginary [ε_2] parts of complex relative permittivity and (b) corresponding complex refractive index [*n*, *k*] of as-deposited amorphous Sb_2Te_3 measured by variable-angle spectroscopic ellipsometry.

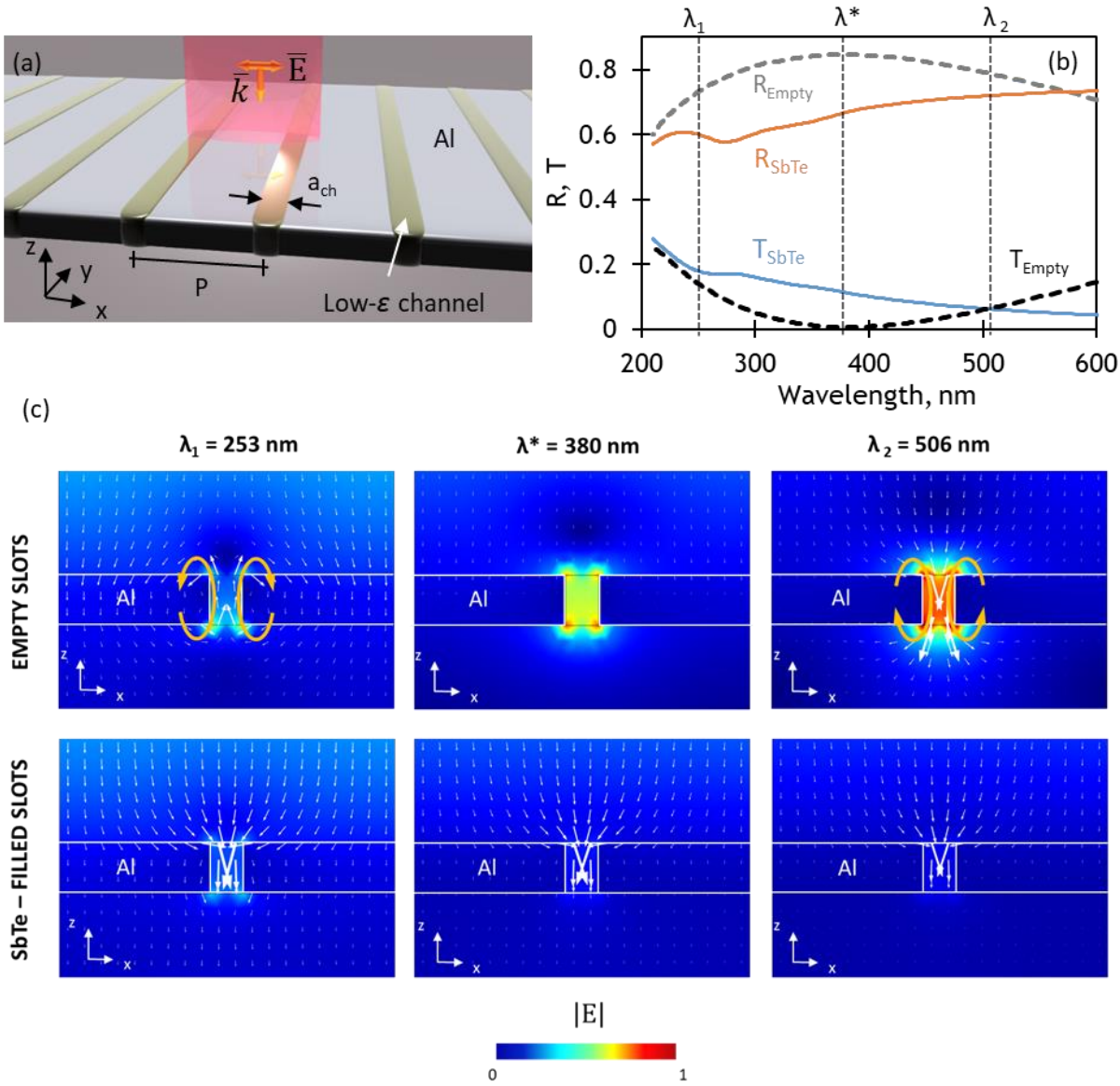

Figure 2. Filling subwavelength apertures in a plasmonic screen with a low-epsilon medium. (a) Schematic illustration of the numerically simulated metasurface, which comprises a periodic array of linear slots (width w << illumination wavelength λ, center-to-center spacing $P < \lambda$) in a semi-transparent aluminum film (thickness t = 15 nm) that may either be empty or, as shown, filled with amorphous Sb_2Te_3. Incident light is polarized perpendicular to the slots. (b) Spectral dispersion of reflection and transmission for a metasurface, of period P = 100 nm and w = 10 nm, with empty and Sb_2Te_3-filled slots [dashed and solid lines respectively]. (c) Spatial distribution of electric field in the xz plane, overlaid with arrows showing net [time-averaged] powerflow, for metasurfaces with empty slots and with Sb_2Te_3-filled [upper and lower rows respectively] at Sb_2Te_3's two ε_1 zero-crossing wavelengths, λ_1 = 253 [left] and λ_2 = 506 nm [right], and at λ^* = 380 nm [center].

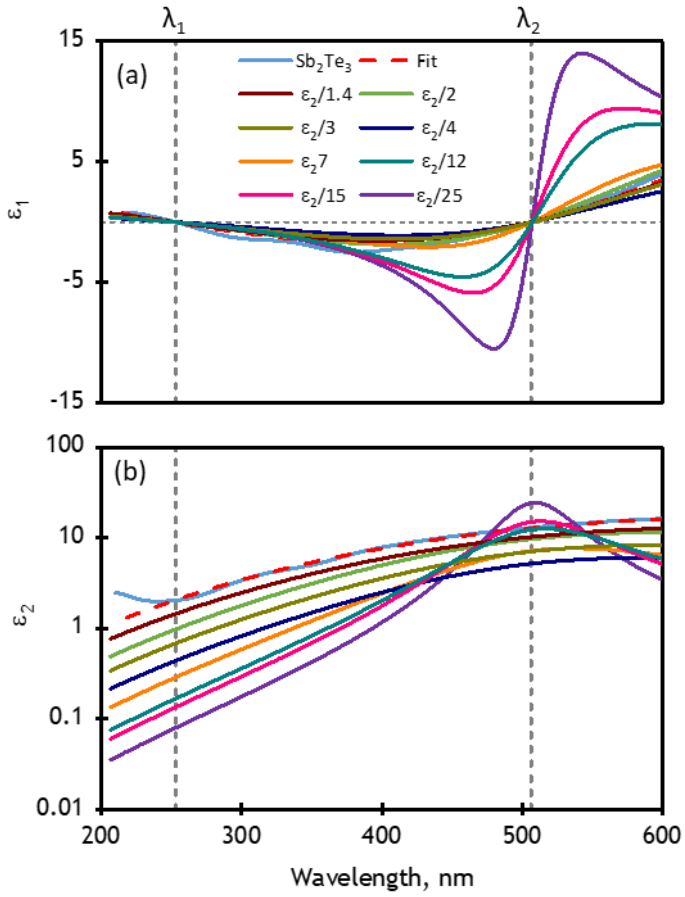

Figure 3. Analytical modelling and modification of antimony telluride's relative permittivity. Lorentzian oscillator fittings [dashed red lines] to the (a) real and (b) imaginary parts of measured relative permittivity for Sb_2Te_3 [as presented in Figure 1a, blue lines]; and Kramers-Kronig-compliant spectral dispersion of complex permittivity for hypothetical media having the same value of ε_1 in the UV range but lower losses: ε_2 reduced by a factors ranging from 1.4 to 25 at the $\varepsilon_1 = 0$ wavelength $\lambda_1 = 253$ nm.

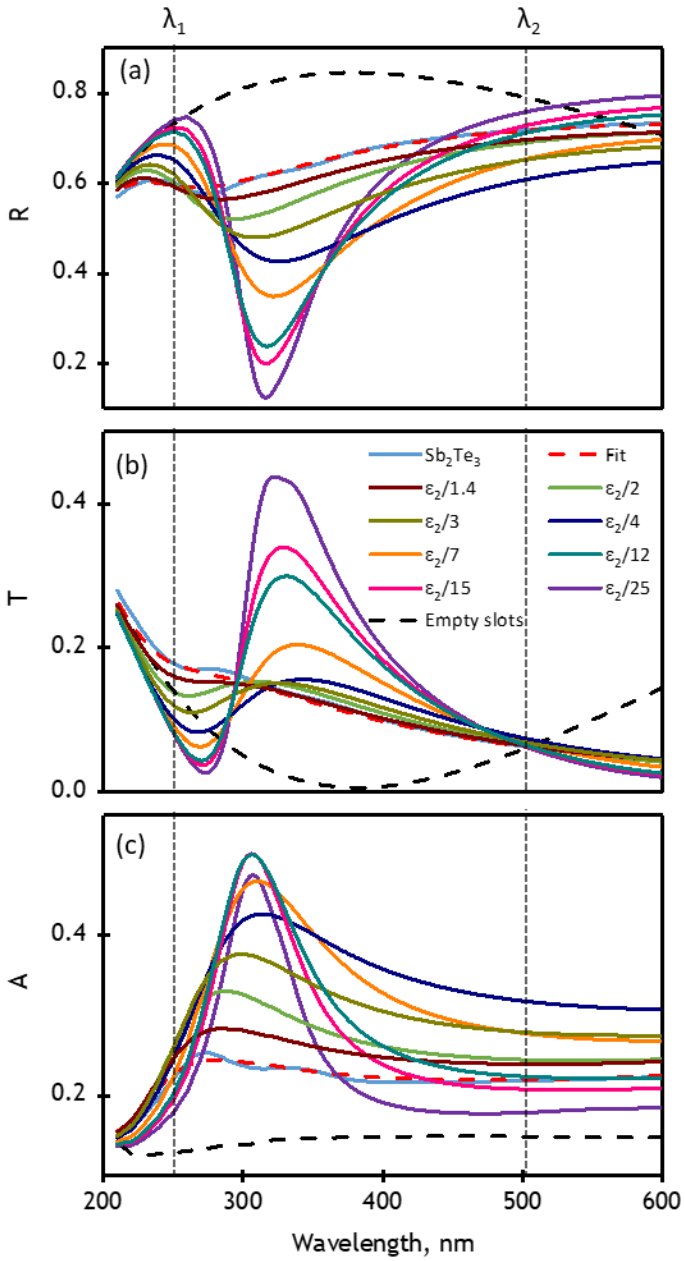

Figure 4. Reduction of losses in low-epsilon composite metasurfaces. Spectral dispersion of (a) reflection, (b) transmission, and (c) absorption for the metasurface of Figure 2b with empty slots [dashed black lines], Sb_2Te_3-filled slots [blue lines and dashed red lines for the corresponding oscillator model fitting], and slots filled with hypothetical reduced-loss variants of the chalcogenide with permittivites as presented in Figure 3 [ε_2 reduction factors between 1.4 and 25 as per Fig. 3].

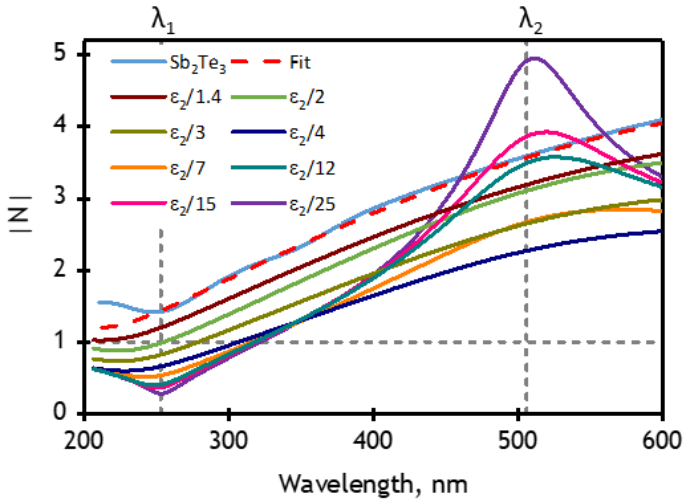

Figure 5. Refractive index of antimony telluride and reduced-loss variants. (a) Spectral dispersion of the magnitude of complex refractive index $N = n + ik$, including traces derived from the experimental data for synthesized Sb_2Te_3 [Figure 1b], the Lorentzian fitting to this data and the hypothetical reduced-loss variants [Figure 3a and b].

'Laminar flow' transmission of light, suppression of plasmonic powerflow vortices, and levels of absorption increasing with decreasing Joule losses can be observed in metamaterials combining plasmonic nanostructures with chalcogenide semiconductor inclusions exhibiting low-epsilon/low-index characteristics.

Keywords: Photonic metamaterial; Chalcogenide; Low-epsilon; Low-index

D. Piccinotti, B. Gholipour, J. Yao, K. F. MacDonald*, B. E. Hayden and N. I. Zheludev

Optical Response of Nano-hole Arrays Filled with Chalcogenide Low-epsilon Media